Applied Thermal Engineering 160 (2019) 113960

Contents lists available at ScienceDirect

Applied Thermal Engineering

journal homepage: www.elsevier.com/locate/apthermeng

Research Paper

Modeling and analysis of thermal runaway in Li-ion cell

Z. An[a,b,1], K. Shah[b,1], L. Jia[a,*], Y. Ma[b,*]

[a] Institute of Thermal Engineering, School of Mechanical, Electronic and Control Engineering, Beijing Jiaotong University, Beijing 100044, China
[b] Mechanical Engineering Department, University of California at Merced, Merced, CA, USA

HIGHLIGHTS

- An analytical model to predict thermal runaway of lithium-ion cells.
- Validation of the model through comparison with experiments and other models.
- Application of the model for the design to prevent thermal runaway.
- Demonstration of an effective tool for thermal runaway analysis and prevention.

ARTICLE INFO

Keywords:
Lithium-ion battery
Thermal runaway
Battery safety
Thermal runaway prevention
Analytical model
Thermal management

ABSTRACT

Thermal runaway is the top safety concern for Li-ion electrochemical energy storage systems. There are multiple abuse conditions that may cause thermal runaway in Li-ion cells. Although thermal runaway has been extensively studied, the runaway mechanisms due to external short circuit and ultra-high discharge rates (> 10C) are relatively less studied. In the present work, an analytical thermal runaway model is developed to predict thermal runaway in prismatic and pouch Li-ion cells due to either external short circuit or ultra-high discharge rates. The heat generation data corresponding to the ultra-high discharge rates considered in the thermal runaway model have been obtained separately using an electrochemical-thermal coupled model. The analytical thermal runaway model is validated against experiments as well as COMSOL, a finite element-based commericial solver. Using the analytical model, the effects of key parameters on cell safety have been analyzed. Finally, the analytical model has been used to evaluate effectiveness of a thermal runaway prevention strategy based on boiling in minichannels of a water-cooled minichannel based battery thermal management system.

1. Introduction

Li-ion cells have been widely used in battery electric vehicles (BEV), hybrid electric vehicles (HEV), plug-in hybrid electric vehicles (PHEV), and stationary energy storage units due to their high specific energy and excellent cycle life [1,2]. However, the safety of Li-ion battery packs has become a key issue, especially under extreme or abuse conditions [3,4]. Fire and explosion due to onset of thermal runaway have been reported [5], often leading to catastrophic damages. Thermal runaway is caused by drastic and successive processes and reactions that feed into one another, eventually, leading to fire and combustion [6]. The pertinent reactions during thermal runaway include decomposition of solid electrolyte interface (SEI), reaction between anode and electrolyte, decomposition of cathode material, and electrolyte decomposition [7,8]. These different reactions, each with different onset temperatures, essentially form a chain of reactions resulting in thermal runaway.

Thermal runaway in Li-ion cells has been widely studied under various abuse conditions such as nail penetration [9,10], thermal abuse [11], mechanical abuse [12,13], overcharge [14] and external short circuit [15]. In addition, the effects of thermal properties and reaction kinetics of cells, both at material and cell level, have also been studied both theoretically and experimentally [16–18]. A simplified one dimensional model has been developed to predict the thermal abuse behavior of Li-ion cells under oven test condition [7]. In addition to the simplified model, various other models have been developed to investigate safety behaviors of Li-ion cell under different abuse conditions, such as nail penetration [20], crushing [21], short-circuiting [22], and overheating [23].

One of the possible scenarios causing thermal runaway is aggressive

* Corresponding authors.
E-mail addresses: ljia@bjtu.edu.cn (L. Jia), yma5@ucmerced.edu (Y. Ma).
[1] These authors contributed equally to this work.

https://doi.org/10.1016/j.applthermaleng.2019.113960
Received 19 December 2018; Received in revised form 6 May 2019; Accepted 15 June 2019
Available online 15 June 2019
1359-4311/

Nomenclature

List of symbols

a	height of channel (mm)
A	thickness of tube (mm)
A_b	superficial area of battery in ZY plane (mm^2)
A_c	superficial area of channels (mm^2)
b	width of channel (mm)
Bl	Boiling number
Bo	Bond number
c_2	Li^+ concentration in liquid phase (mol m^{-3})
C_p	heat capacity (J kg^{-1} K^{-1})
D_h	hydraulic diameter (mm)
E_a	activation energy (J mol^{-1})
$f_\pm$	average molar activity coefficient
F	Faraday constant (C mol^{-1})
g	gravitational acceleration (m s^{-2})
G	mass flux in the channels (kg m^{-2} s)
h	convection heat transfer coefficient (W m^{-2} K^{-1})
h_c	convection heat transfer coefficient in the channels (W m^{-2} K^{-1})
h_b	effective convection coefficient on cell surface (W m^{-2} K^{-1})
h_{fg}	latent heat of water (J kg^{-1})
H	height of the cell (mm)
j_{loc}	local current density (A m^{-2})
k	thermal conductivity (W m^{-1} K^{-1})
k_{al}	thermal conductivity of aluminum (W m^{-1} K^{-1})
k_w	thermal conductivity of water (W m^{-1} K^{-1})
k_x	thermal conductivity of cell in X direction (W m^{-1} K^{-1})
L	length of the cell (mm)
$\dot{m}$	mass flow rate (kg s^{-1})
N	number of channels in the tube
Nu	Nusselt number
q_b	heat flux on cell surface (W m^{-2})
q_c	heat flux on the wall of channels (W m^{-2})
Q_0	pre-exponential constant (W m^{-3})
Q_{act}	active polarization heat generation (W m^{-3})
Q_e	electrolyte decomposition heat (W m^{-3})
$Q_{exothermic}$	material decomposition heat generation in the cell (W m^{-3})
Q_{ne}	negative-electrolyte reaction heat (W m^{-3})
$Q_{nominal}$	nominal heat generation in the cell (W m^{-3})
Q_{ohm}	ohmic heat generation (W m^{-3})
Q_{pe}	positive-electrolyte reaction heat (W m^{-3})
Q_{rea}	reaction heat generation (W m^{-3})
Q_{sei}	SEI decomposition heat (W m^{-3})
R	universal gas constant (J mol^{-1} K^{-1})
Re_l	liquid Reynolds number
S_a	specific surface area (m^2 m^{-3})
ΔS	entropy change (J mol^{-1} K^{-1})
t	time (s)
t_+	Li^+ transference number
t_f	half thickness of the fin (mm)
T	absolute temperature (K)
T_∞	ambient temperature (K)
U	electric potential (V)
W	width of the cell (mm)
x_e	vapor quality in channels at outlet

Greek letters

β	slope of $Q_{exothermic}$
η	overpotential (V)
η_f	fin efficiency
θ	temperature increase (K)
μ_l	dynamic viscosity of saturated liquid (Pa s)
μ_n	Eigenvalues
ρ	density (kg m^{-3})
ρ_l	density of saturated liquid (kg m^{-3})
ρ_g	density of saturated vapor (kg m^{-3})
σ	surface tension (N m^{-1})
σ_1	electric conductivity for solid phase (S m^{-1})
σ_2	electric conductivity for liquid phase (S m^{-1})
φ_1	solid phase potential (V)
φ_2	liquid phase potential (V)

cell discharging at an ambient temperature as high as 60 °C or under poor heat dissipation conditions [4].The higher discharge can be required by an application or due to an external short circuit. Some numerical simulation and experimental studies of external short circuit can be found in the literature [15,22,24]. Heat generation rate in a 26650 cylindrical Li-ion cell has been measured for discharge rates up to 9.6C [25]. The measurement of heat generation rate and temperature distribution on the surface of a large format Li-ion pouch cell over a wide range of operating temperatures (−10 °C to 50 °C) and discharge rates (0.5C–10C) have also been reported [26]. However, there is very limited work reported on thermal modeling of Li-ion cells discharged at much higher discharge rates, especially under conditions which may lead to thermal runway [27]. During such high discharge operation, a significant amount of heat is generated in the cell [25]. Consequently, the temperature of the cell may become high enough to trigger decomposition reactions, causing a chain of reactions ultimately leading to thermal runaway and explosion. In the event of initiation of decomposition reactions, exothermic reactions contribute significantly to the overall heat generation of the cell. The reaction rate for these reactions follow Arrhenius reaction kinetics. This may cause the overall heat generation in the cell to increase exponentially with temperature. Since the heat removal rate from the surface of the cell due to convection only increases linearly with temperature, the temperature of the cell may increase rapidly under such conditions. In addition to heat dissipation from the surface by convective heat transfer, heat conduction within the cell is also of critical importance. Poor heat conduction within the cell can limit the heat removal rate from the core of the cell. This can lead to a very large thermal gradient within the cell making external cooling ineffective. Hence, it is critical to analyze the effect of heat conduction within the cell while modeling thermal transport during abuse conditions. Multiphysics models are necessary to capture the coupled nature of electrochemical reactions and thermal transport processes, which can be applied for the prediction of temperature fields as well as optimizing the design of thermal management systems to enhance Li-ion battery safety.

In the present work, a framework consisting electrochemical-thermal coupled model and analytical thermal runaway model has been developed and applied to predict thermal runaway at ultra-high discharge conditions. The effects of discharge rate, operating temperature, out-of-plane thermal conductivity, and thickness of the cell have been analyzed using this framework. Finally, using the same framework, boiling heat transfer in the minichannels for the water-cooled minichannel based battery thermal management has been studied as a possible strategy to prevent thermal runaway at cell and pack level.

2. Mathematical modeling

As shown in Fig. 1, a $LiFePO_4$ pouch/prismatic Li-ion cell with

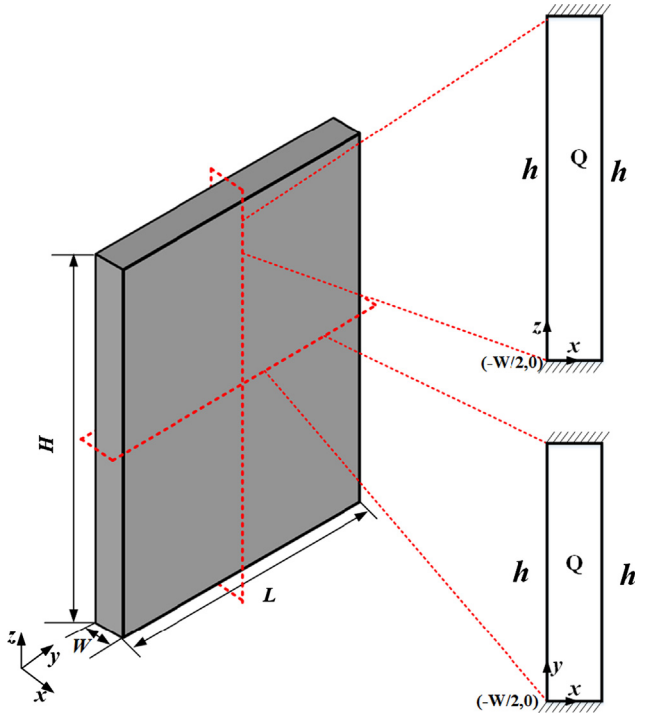

Fig. 1. Schematic of Li-ion pouch cell along with two cross sections showing applicable boundary conditions.

width W, length L, and height H is considered. The two faces of the cell in the YZ plane experience convective heat transfer with convective heat transfer coefficient h. The orthotropic nature of head conduction inside the cell is considered. Since the cell surface in the XZ and XY plane only experiences natural convection and the thermal conductivity in the in-plane direction is much larger than in the out-of-plane direction, the Biot number in the in-plane direction is much less than one ($Bi < < < 1$). This indicates uniform temperature and negligible heat transfer in the in-plane direction within the cell. Therefore, the three-dimensional heat transfer problem can be reduced to one-dimensional heat transfer along the out of plane direction for thermal runaway modeling. Similar simplification has also been made and justified in a past work where heat transfer in a Li-ion cell is reduced to a two dimensional problem [28].

2.1. Electrochemical-thermal coupled model

The heat generation due to ohmic heat, active polarization heat, and entropic heat have been calculated using the electrochemical-thermal coupled model. The heat generation from these different mechanisms is expressed in Eqs. (1)–(4) [29,30],

$$Q_{nominal} = Q_{rec} + Q_{act} + Q_{ohm} \tag{1}$$

$$Q_{rea} = S_a j_{loc} T\frac{\partial U}{\partial T} = S_a j_{loc} T\frac{\Delta S}{F} \tag{2}$$

$$Q_{act} = S_a j_{loc} \eta \tag{3}$$

$$Q_{ohm} = \sigma_1^{eff} \nabla\varphi_1 \cdot \nabla\varphi_1 + \left[\sigma_2^{eff} \nabla\varphi_2 - \frac{2RT\sigma_2^{eff}}{F}\left(1 + \frac{\partial \ln f_{\pm}}{\partial \ln c_2}\right)(1 - t_+)\nabla(\ln c_2)\right] \cdot \nabla\varphi_2 \tag{4}$$

Here, Q_{rec}, Q_{act}, and Q_{ohm} correspond to heat generation from electrochemical reactions, active polarization, and Ohmic heating, respectively. $Q_{nominal}$ is the total heat generation in the cell due to the discharge process. The above equations are solved by the electrochemical-thermal coupled model using the COMSOL Multiphysics solver. Details about this model can be found in recent articles [31,32]. At very high discharge rates ($\geq$10C), as considered in the present work, Ohmic heat generated due to electrical contact resistances in the cell becomes significant. Hence, electrical contact resistances reported in the literature are considered in the model [33]. Although the nominal heat generation defined by Eqs. (1)–(4) varies with depth of discharge, an averaged value over the duration of discharge has been calculated and used in the thermal runaway model.

2.2. Analytical thermal runaway model

An analytical thermal runaway model is developed using the nominal heat generation as calculated from the electrochemical-thermal coupled model to predict the temperature and the onset of thermal runaway in a Li-ion cell experiencing external short circuit/ultra-high discharge rates. Exothermic heat due to material decomposition processes is accounted for in the analytical model. Four key decomposition processes: SEI decomposition, negative-electrolyte reaction, positive-electrolyte reaction, and electrolyte decomposition are considered. The total exothermic heat due to these reactions is given by,

$$Q_{exothermic} = Q_{sei} + Q_{ne} + Q_{pe} + Q_e \tag{5}$$

Heat generation due to these material decompositions follows Arrhenius kinetics and can be expressed in its generic form by,

$$Q = Q_0 \exp\left(-\frac{E_a}{RT}\right) \tag{6}$$

where Q_0 is the pre-exponential constant, R is the ideal gas constant, and E_a is the activation energy. Details on these different decompositions can be found in the literature [19,34].

The $Q_{exothermic}$ term is linearized and a piecewise linear approximation is considered in solving the governing energy equation as shown below,

$$k\frac{\partial^2\theta}{\partial x^2} + Q_{nominal} + \beta(\theta + T_\infty) = \rho C_p \frac{\partial\theta}{\partial t} \tag{7}$$

$$\frac{\partial\theta}{\partial x} = 0 \text{ at } x = 0 \tag{8}$$

$$-k\frac{\partial\theta}{\partial x} = h\theta \text{ at } x = \frac{W}{2} \tag{9}$$

$$\theta = 0 \text{ at } t = 0 \tag{10}$$

where

$$\theta = T - T_\infty \tag{11}$$

$$\beta = \frac{Q_{exothermic}}{(\theta + T_\infty)} \tag{12}$$

Here, β is a coefficient to be multiplied with the absolute temperature to obtain the exothermic heat generation at that temperature. This coefficient is calculated and updated in the equation to ensure that the piecewise linear approximation of $Q_{exothermic}$ with respect to temperature closely follows the actual non-linear temperature-dependent nature of this heat generation term. The solution to Eqs. (7)–(10) is obtained analytically by first splitting the solution of θ into two sub-problems resulting in an ordinary differential equation and a partial differential equation. Then, both these differential equations are solved analytically to compute temperature as given by the final solution below,

$$\theta = s(x) + w(x, t) \tag{13}$$

The solution to the ordinary differential equation is given by,

$$s(x) = A\left(\sin(\sqrt{\beta/k}x) + \frac{\sqrt{\beta k}}{h}\cos(\sqrt{\beta/k}x)\right) + \frac{Q_{no\,min\,al}}{\beta}(\cos(\sqrt{\beta/k}x) - 1) \tag{14}$$

where

$$A = \frac{Q_{no\,min\,al}\left(\frac{\sin(\sqrt{\beta/k}W)}{\sqrt{\beta/k}} - \frac{h}{\beta}(\cos(\sqrt{\beta/k}W) - 1)\right)}{\left(h - \frac{\beta k}{h}\right)\sin(\sqrt{\beta/k}W) + 2\sqrt{\beta k}\cos(\sqrt{\beta/k}W)} \tag{15}$$

The partial differential equation is solved by the separation of variables method. The solution is given by,

$$w(x,t) = \sum_{n=1}^{\infty} A_n\left(\cos(\mu_n x) + \frac{h}{k\mu_n}\sin(\mu_n x)\right)e^{-\left(\mu_n^2 - \frac{\beta}{k}\right)\alpha t} \tag{16}$$

where

$$A_n = \frac{\int_{x=0}^{W}(T_i(x) - s(x))\cdot\left(\cos(\mu_n x) + \frac{h}{k\mu_n}\sin(\mu_n x)\right)dx}{\int_{x=0}^{W}\left(\cos(\mu_n x) + \frac{h}{k\mu_n}\sin(\mu_n x)\right)^2 dx} \tag{17}$$

Here, coefficients A_n, as defined by Eq. (17), are to be recalculated as the value of β changes in Eq. (7) to maintain accuracy of the piecewise linear approximation of $Q_{exothermic}$. To recalculate A_n, T_i in Eq. (17) is updated to the temperature field at the final time step using the previous value of β. Since the calculation of coefficients A_n is computationally intensive, the value of β is calculated and updated in the model such that accuracy of the solution is not compromised in a computationally efficient manner. Determination of β requires calculating the total exothermic heat due to the four key decomposition reactions. These decomposition reactions are governed by Arrhenius reaction kinetics. The exothermic heat released during these reactions is proportional to the reaction rate for these reactions which is obtained by solving the corresponding ordinary differential equations. The present framework includes these calculations in order to calculate β. More details about these reactions and parameters can be found in some of the past works on thermal runaway modeling and simulations [19,34–36].

The eigenvalues μ_n in Eqs. (16) and (17) are calculated by solving the following transcendental equation,

$$\tan(\mu_n W)\cdot\left(k\mu_n - \frac{h^2}{k\mu_n}\right) - 2h = 0 \tag{18}$$

2.3. Effective convective heat transfer coefficient for boiling heat transfer

Using the analytical model, the effectiveness of boiling heat transfer in minichannels of a water-cooled minichannel based battery thermal management for thermal runaway prevention is analyzed. The coolant is passed through a cold plate consisting of minichannels as shown in the schematic of the thermal management system provided in supplementary Fig. 1. The cold plate is in contact with the large face (YZ plane) of the cell on both sides. The coolant considered in this analysis is deionized water. The parameters relevant to this study are provided in Table 1.

Correlations for boiling heat transfer in water flowing in a minichannel are widely available in the literature. The following boiling heat transfer correlation to calculate convective heat transfer coefficient is used in the analytical model [37],

$$Nu = 334Bl^{0.3}(BoRe_l^{0.36})^{0.4} \tag{19}$$

The Bl, Bo and Re_l are boiling number, Bond number, and liquid Reynolds number, respectively, which are defined as below,

$$B\,l = q_c/(G\mathrm{h_{fg}}) \tag{20}$$

$$Bo = g(\rho_l - \rho_g)D_h^2/\sigma \tag{21}$$

$$Re_l = G(1 - x_e)D_h/\mu_l \tag{22}$$

The thermodynamic vapor quality at the outlet (x_e) is defined as,

$$x_e = q_c \times A_c/\dot{m}h_{fg} \tag{23}$$

Here, q_c is the heat flux on the minichannel walls which is calculated using the temperature gradient at the cell surface obtained using the analytical model. This heat flux is given by,

$$q_c = -k_x\frac{d\theta}{dx}\cdot\frac{A_b}{A_c} \tag{24}$$

where A_c and A_b are the minichannel and cell surface area respectively. They are expressed as,

$$A_c = \mathrm{N} \times \mathrm{b} + 2 \times (N - 1) \times (\mathrm{a}+t) \times \eta_f \tag{25}$$

$$A_\mathrm{b} = \mathrm{H} \times \mathrm{L} \tag{26}$$

The fin effect in the minichannel is considered accounting for fin efficiency given by,

$$\eta_f = \frac{\tanh(m(a + (A - a)/4))}{m(a + (A - a)/4)} \tag{27}$$

where

$$m = \sqrt{\frac{h_c \times (L + 2 \times t_f)}{k_{al} \times L \times t_f}} \tag{28}$$

Due to high thermal conductivity of aluminum and small minichannel wall thickness, it's reasonable to ignore thermal resistance due to the minichannel wall in calculating the effective convective heat transfer coefficient. The heat transfer coefficient on the minichannel wall (h_c) and cell surface (h_b) is calculated as below,

$$h_\mathrm{c} = N\,\mathrm{u}\times k_\mathrm{w}/D_h \tag{29}$$

$$h_\mathrm{b} = h_\mathrm{c} \times A_\mathrm{c}/A_\mathrm{b} \tag{30}$$

In the analytical model, eigenvalues are recalculated by solving Eq. (18) as the value of effective convective heat transfer coefficient in Eq. (30) changes due to boiling. This would also require recalculating coefficients A_n in Eq. (17). Hence, similar to β, convective heat transfer coefficient should be changed in the analytical model such that temperature can be computed with sufficient accuracy without increasing the computational effort unnecessarily.

3. Model validation

3.1. Electrochemical-thermal coupled model validation

The nominal heat generation computed using the electrochemical-thermal coupled model is compared with the experimental measurements for discharge rates up to 10C. The heat generation from the coupled model and measurements reported in the literature for a cylindrical 2.6 Ah $LiFePO_4$ 26650Li-ion cell [25] are plotted in Fig. 2 at different discharge rates. There is good agreement between the heat

Table 1
Dimensions related to Li-ion cell, minichannel, and tube.

Properties	Parameters
H (mm)	200
L (mm)	140
W (mm)	7
A (mm)	3
a (mm)	2
b (mm)	2

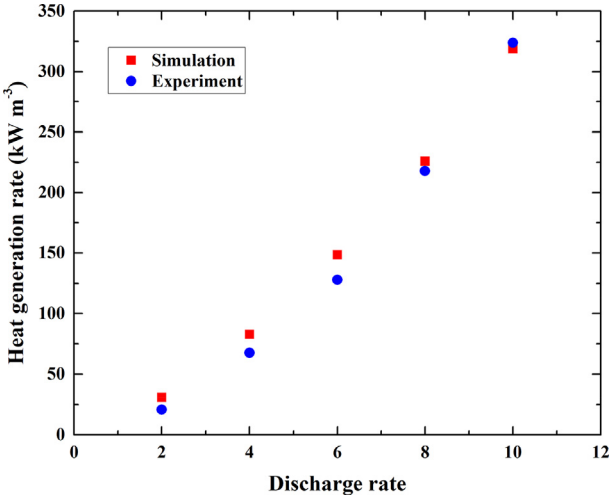

Fig. 2. Comparison of heat generation rates calculated from the electro-chemical-thermal model with experimental values reported for different discharge rates [25].

generation calculated from the coupled model and experimental measurements. It should be noted that the heat generation from the simulations is averaged over the duration of discharge. Due to lack of experimental data on heat generation measurement at discharge rates higher than 10C, heat generation calculated using this model is be used in the thermal runaway analysis.

3.2. Analytical model validation

The analytical thermal runaway model has been validated with an experimentally validated model from a past work [7]. The model reported in the past work had been experimentally validated for an 18650 cylindrical Li-ion cell. Due to limited work on thermal runaway measurement on prismatic and pouch cells, direct experimental validation of the analytical model has not been obtained.

Due to the approximations involved in accounting for temperature dependent heat generation during thermal runaway and heat flux dependent convective heat transfer coefficient due to boiling in minichannel, the analytical model is validated against finite-element based solver COMSOL Multiphysics.

3.2.1. Validation with past work

In the past work, the experimentally validated thermal runaway model had been used to predict temperature of a prismatic cell during oven test [7]. All the parameters used in the analytical model are provided in the past work [7].

Two prismatic cells, Cells A and B with thicknesses 15 mm and 3.6 mm, respectively, are considered in the study. Cell surface temperatures have been predicted using the analytical model for both of the cells during the oven test. Oven temperatures of 140 °C and 160 °C are considered. As shown in Fig. 3, Cell A doesn't enter thermal runaway for oven temperature 140 °C but enters thermal runaway for oven temperature 160 °C. On the other hand, Cell B doesn't enter thermal runaway even for oven temperature 160 °C. Surface temperature of Cell B overshoots slightly above the oven temperature of 160 °C. This has also been observed in the past work used for validation. In Fig. 3, surface temperature of Cell A and B as predicted using the analytical model and the experimentally validated model from the past work are plotted. There is excellent agreement between the two models.

3.2.2. Numerical validation

To validate the thermal runaway aspect of the model, a COMSOL simulation is conducted with same parameters as used in the analytical model for oven test simulation. Temperature at the surface of the cell is plotted against time from the analytical model and COMSOL Multiphysics in Fig. 4. Two different oven temperatures are considered for the validation. There is good agreement between the two models for both the oven temperatures considered. This validation shows that the piecewise linear approximation used in the analytical model doesn't affect the accuracy of the solution as no such approximation is used in the COMSOL simulation. The analytical model is also found to be significantly faster than the COMSOL simulation.

In addition to the thermal runaway aspect, the analytical model is validated against COMSOL Multiphysics considering boiling effect in minichannel using the phase-change heat transfer correlation described earlier. For this validation, temperature-dependent heat generation in the Li-ion cell during thermal runaway is not considered. Instead, a very high constant heat generation rate of 1000 kW/m^3 is considered in the cell. This will create sufficient boiling effect in order to do the validation under a wide range of heat flux and convective heat transfer coefficient. Temperature predicted from both the analytical model and COMSOL Multiphysics simulation are plotted in Fig. 5. There is excellent agreement between the two models. This indicates that the analytical model is capable of accurately predicting temperature when boiling effect is considered.

4. Result and discussion

4.1. The effect of operating condition

There are multiple design and operation parameters of the Li-ion cell such as discharge rate, operating temperature, cell thickness, and thermo-physical properties which can affect their performance, life-cycle, and safety. In general, these parameters directly determine the heat generation and removal rate of the cell, which in turn determine the temperature and safety of the cell. In order to understand the effect of these design and operation parameters on the safety of cells, temperature and thermal runaway predictions for cells under different conditions have been performed using the analytical model.

In Fig. 6(a), temperature prediction for different discharge rates is presented. The ambient temperature considered is 30 °C. The discharge rate is varied in the range 12–25C. As shown in the figure, even a high discharge rate of up to 15C may not result in thermal runaway under the conditions considered in this analysis. The out-of-plane thermal conductivity and convective heat transfer coefficient considered are

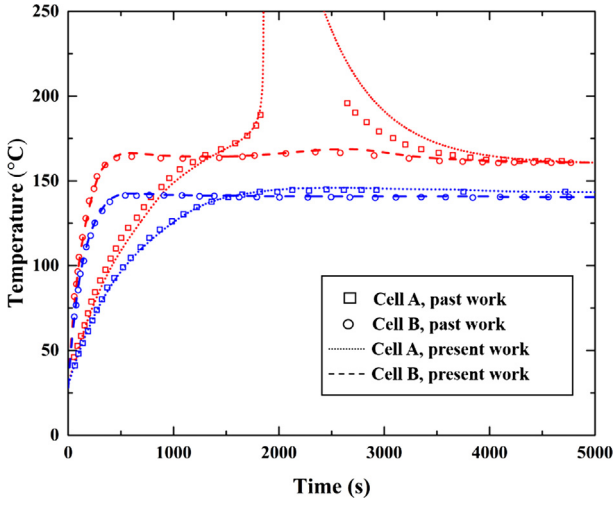

Fig. 3. Comparison of Temperature as a function of time predicted by the analytical model and past work [7] during an oven test with oven temperature 140 °C (Blue) and 160 °C (Red). (For interpretation of the references to colour in this figure legend, the reader is referred to the web version of this article.)

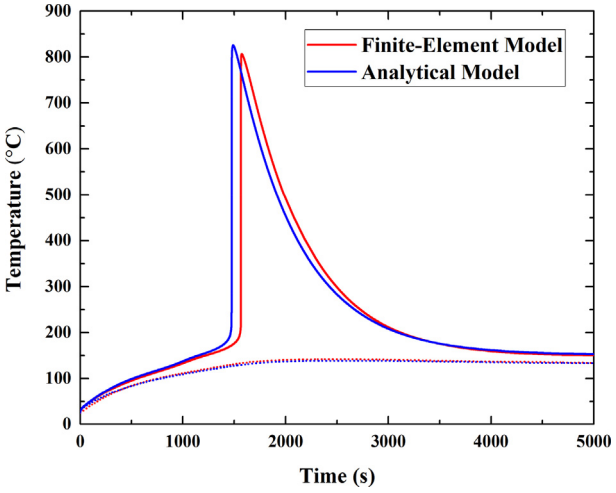

Fig. 4. Comparison of temperature as a function of time predicted by the analytical model and finite-element simulations for oven temperatures 140 °C (Dashed line) 150 °C (Solid line).

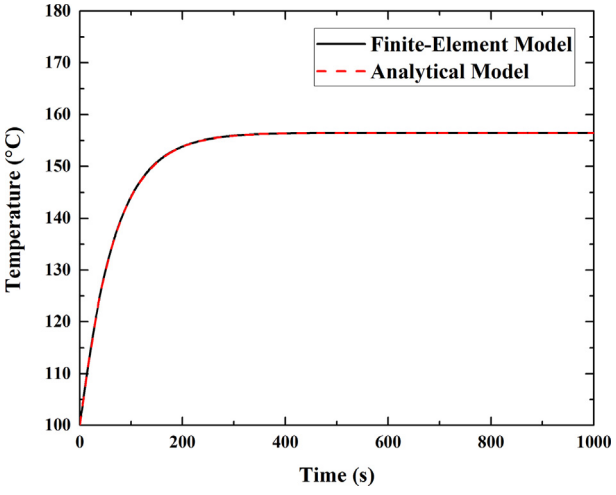

Fig. 5. Comparison of the core temperature of the cell calculated from finite-element model and analytical model considering effect of boiling heat transfer in minichannels.

0.25 W/mK and 5 W/m^2 K, respectively. Heat generation due to Ohmic, over-potential, and entropic heat during different discharge rates are calculated using the electrochemical-thermal coupled model. If this heat generation doesn't increase the temperature of the cell enough to initiate the chain of reactions of different decompositions, as in the case for 12C and 15C discharge rates in the present analysis, thermal runaway may not occur. On the other hand, for discharge rates higher than 15C, the chain reactions consisting of different decompositions occurs ultimately leading to thermal runaway. In addition to discharge rate, the ambient temperature at which the cell is being discharged also affects safety of the cell. The ambient temperature is varied in the range 20 °C-60 °C and the prediction of core temperature in the cell discharging at 15C is presented in Fig. 6(b). As seen in the figure, ambient temperatures less than 30 °C don't result in thermal runaway which is consistent with the results from Fig. 6(a). However, ambient temperatures of 40 °C or higher result in thermal runaway as per the model prediction. Here, as the ambient temperature increases, the convective heat transfer between the cell and the surroundings reduces. This causes the temperature of the cell to increase enough to trigger the chain reaction involving decomposition of different materials in the cell leading to thermal runaway. A more detailed analysis of occurrence of thermal runaway can be done by analyzing different decomposition processes involved as presented below.

In Fig. 7(a) and (b), the degree of decomposition and reaction during different reactions is shown in terms of non-dimensional parameters. Discharge rates of 15C and 18C are considered for the results presented in Fig. 7(a) and (b), respectively. Ambient temperature is considered to be 30° for this analysis. For the discharge rate of 15C, only SEI decomposition takes place, which results in a very limited amount of heat generation. The total heat generation and temperature increase for this case is insufficient to trigger subsequent decompositions and reactions. For the higher discharge rate of 18C, in addition to SEI decomposition, the reaction between the negative electrode and solvent is triggered. The total heat generation in this case causes temperature to increase enough to initiate a chain reaction ultimately leading to thermal runaway.

Based on the above discussion, the effects of operation parameters such as discharge rate and ambient temperature directly affect the safety of the cell. Therefore, it is of interest to determine conditions under which the cell can operate safely. The thermal runaway model is used to determine safe-unsafe region in the discharge rate and ambient temperature space under different convective cooling conditions as showed in Fig. 8. As expected, if discharge rate is to be increased, the ambient temperature must be decreased to ensure safe operation. Alternatively, the cell can be safely discharged at a higher rate at high

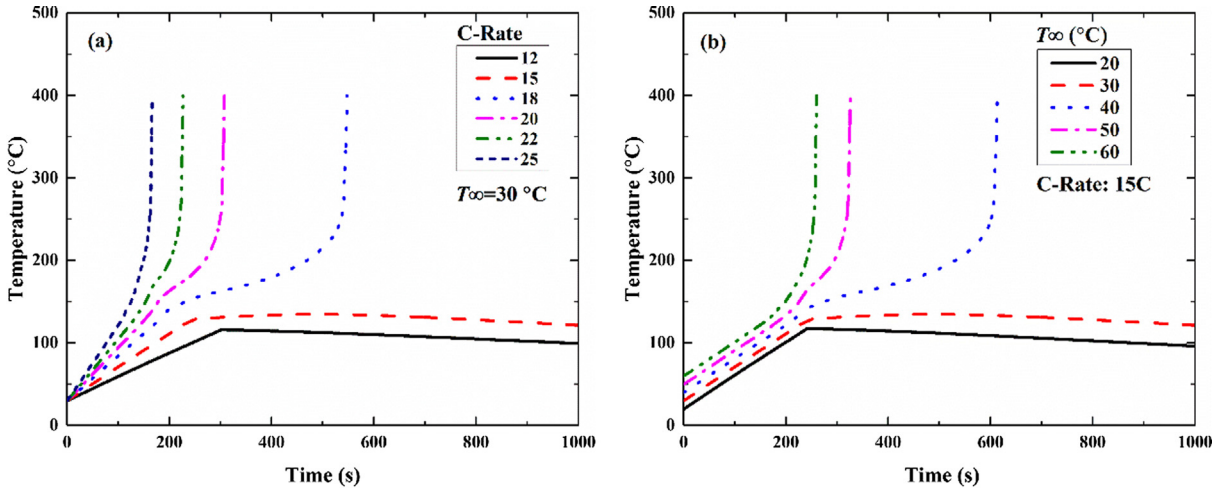

Fig. 6. Core temperature of the cell for (a) different discharge rate (b) different initial/ambient temperature.

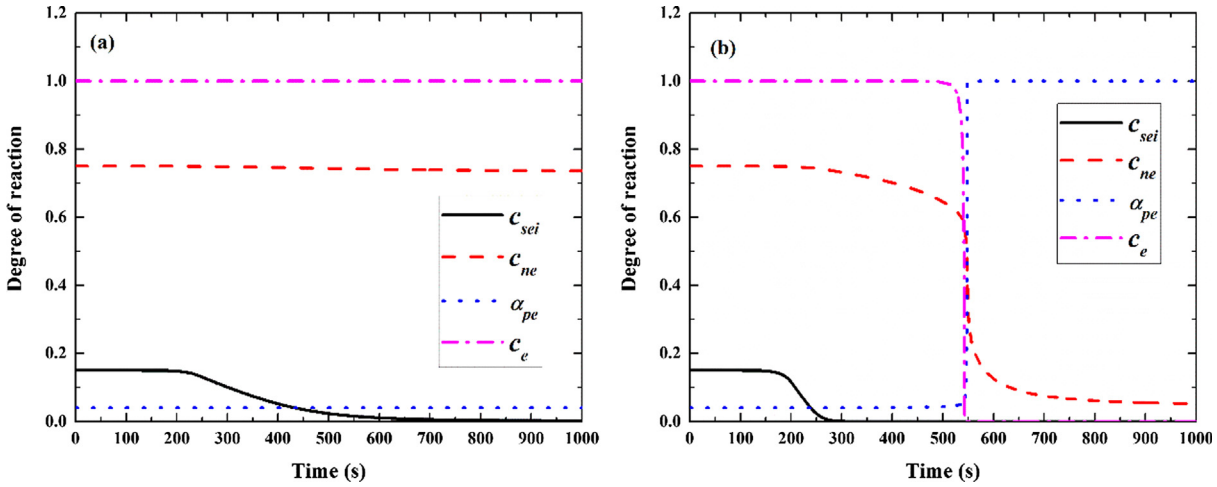

Fig. 7. Evolution of degree of decomposition and reaction for the cell discharged at (a) 15C (b) 18C.

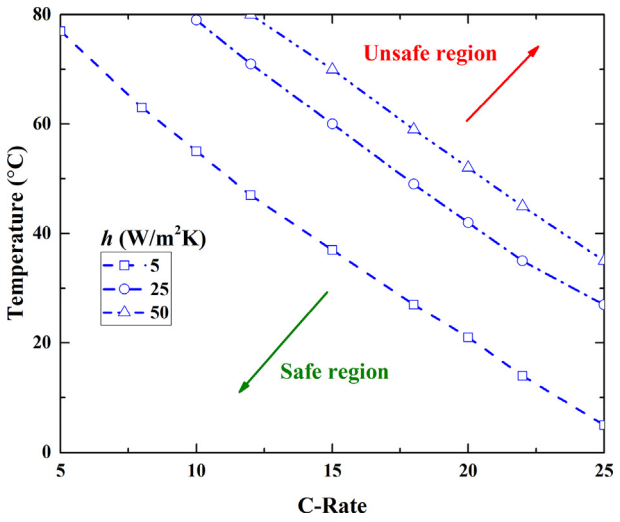

Fig. 8. Temperature to show the safe and unsafe region for cell discharge at different C-rate and operating temperature.

ambient temperature by increasing convective heat transfer up to some extent.

4.2. Effect of cell parameters

Heat removal from a Li-ion cell is determined by heat transfer within the cell body to the cell surface by heat conduction and from the cell surface to the coolant by heat convection. Thermal conductivity of the cell in the out-of-plane direction is poor as heat from the core of the cell must pass through layers of electrodes, electrolyte and interfaces [38,39]. In comparison, the in-plane thermal conductivity can be much larger. Due to the way cells are constructed, typically, a large surface area is available for heat transfer from cell to coolant along the out-of-plane direction. This makes the poor out-of-plane thermal conductivity and cell thickness of significant importance. In Fig. 9(a), the effect of out-of-plane thermal conductivity on the thermal response of the cell has been analyzed. Cell thickness of 15 mm and natural convection condition is considered as thermal conductivity of the cell is varied in the range 0.15–0.45 W/mK. Discharge rate of 15C is considered in this analysis. Thermal state of the cell is found to be very sensitive to the out-of-plane thermal conductivity. A small increase in thermal conductivity may change operation of the cell from being unsafe to safe. As shown in the figure, thermal conductivity of 0.25 W/mK results in thermal runaway which may be prevented with a slightly higher thermal conductivity of 0.35 W/mK. This type of behavior can be understood in terms of effect of thermal resistance on the thermal gradient

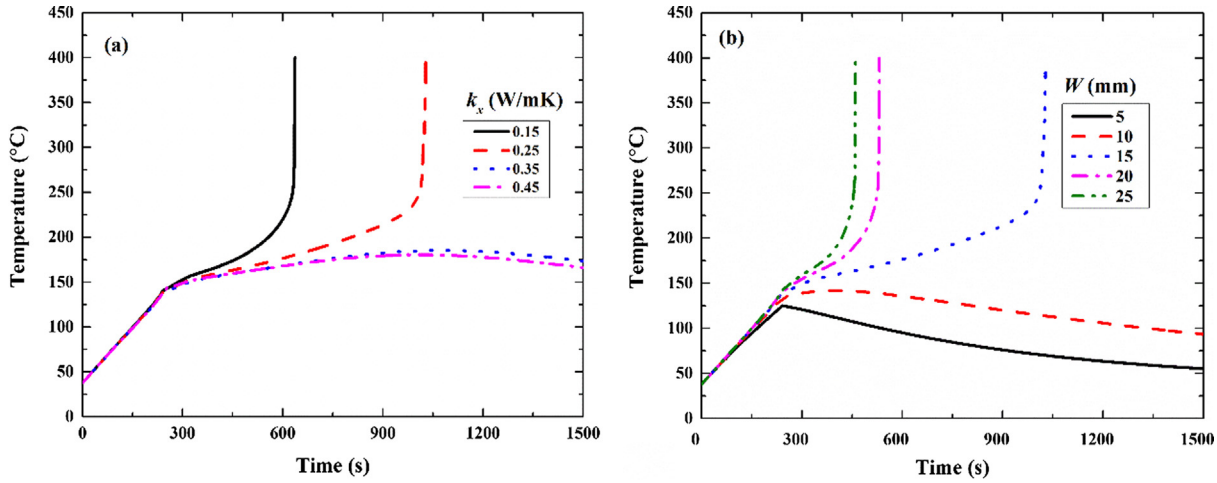

Fig. 9. Core temperature of the cell for (a) different thermal conductivity and (b) different cell thickness.

and core temperature of the cell, which if high enough may trigger chain reaction causing thermal runaway. There have been a few studies demonstrating the possibility of enhancing cell thermal conductivity [40,41]. This analysis clearly shows effectiveness of such an approach to improve the safety of Li-ion cells. In addition to thermal conductivity, cell thickness is also a key parameter affecting thermal resistance of the cell. The effect of cell thickness on the temperature of the cell is shown in Fig. 9(b). A cell thermal conductivity of 0.25 W/mK is considered in this analysis. Convective heat transfer coefficient and discharge rate are kept the same as in the analysis presented in Fig. 9(a). As per this analysis, a cell with thickness 15 mm or higher may not be safe under the conditions considered. However, under the same conditions, cell thickness of 10 mm or less would result in safe operation. This analysis outlines the critical importance of design optimization of the cell as thin cells would be able to withstand harsher conditions than thick cells. On the other hand, the number of cells required would go up if thin cells are used, which would lead to tradeoffs between reliability, safety, cost, and system level complexity.

4.3. Thermal runaway prevention by boiling heat transfer in minichannel

Thermal runaway prevention at the cell level and prevention of thermal runaway propagation at the pack level are key to designing safe energy storage system. One possible way to achieve this is to have a thermal management system specifically designed to both absorb the large amount heat generated in a Li-ion cell at elevated temperature and keep the temperature of the cell below the critical value. Boiling of liquid coolant in minichannel based thermal management system is considered in the present work for this purpose. Since studying the effectiveness of boiling heat transfer in minichannel to suppress thermal runaway is of interest, the case considered in the model is simplified with the proposed thermal management coming in effect at elevated temperatures only. The coolant considered in this study is water due to its boiling point and high latent heat of vaporization. The latent heat of vaporization for water is almost one order of magnitude higher than the required sensible heat to raise the water temperature from room temperature to the boiling point (100 °C). Therefore, sensible heating of water in the minichannel up to the boiling temperature is not considered. Since the thermal management is considered to come in effect only at elevated temperatures, natural convection is considered until surface temperature of the cell rises to 100 °C. Thereafter, boiling heat transfer in the minichannel and resulting convective heat transfer coefficient is considered. Such a scenario significantly simplifies the modeling process and allows studying effectiveness of boiling heat transfer exclusively. To account for boiling effect in the model, the effective convective heat transfer coefficient is calculated as described in Section 2.3. This effective convective heat transfer coefficient is used in the boundary condition of the analytical model described in the Section 2.2. All of the thermal and physical properties of the saturated water under standard atmospheric pressure are acquired from NIST REFPROP 9.0 [42]. As the core temperature of the cell increases with time, the heat generation in the cell increases due to various reactions taking place inside the cell. With increase in heat generation and core temperature, heat transfer from the core to surface increases, which leads to a very high heat dissipation rate due to the boiling of the coolant in the minichannels. The high heat dissipation rate can help restrict the temperature of the core from reaching certain threshold temperature at which chain of reactions initiates. In Fig. 10, prediction of temperature using the analytical model is presented for three different cooling conditions. For both natural and forced convective conditions, the temperature of the cell reaches the threshold value which initiates a chain of reactions ultimately leading to thermal runaway. As expected, under forced convection, onset of thermal runaway occurs a bit later in comparison to natural convection. However, the increase in heat dissipation due to forced convection is not enough to prevent occurrence of thermal runaway. For the thermal management-based approach, once the temperature of the cell surface reaches 100 °C, thermal management based on boiling in minichannel comes into effect. This causes the effective convective heat transfer coefficient on the cell surface to increase dramatically. As a result, complete decomposition and chain reaction are avoided, leading to possibly limited damage to the cell and preventing thermal runaway as well. Based on the flow rate considered in this study, the dryness factor of the water stays reasonably low, avoiding dry-out in the minichannels. Also, the convective heat transfer coefficient is found not to vary significantly with change in dryness factor within the range relevant to the present analysis. Therefore, the convective heat transfer coefficient won't vary significantly along the flow direction under the conditions considered. This allows using an averaged valued of convective heat transfer coefficient at the cell surface. In this analysis, ambient temperature is considered to be 60 °C. The thickness of cell is 10 mm and the out of plane thermal conductivity is 0.25 W/mK. A discharge rate of 25 °C is considered and a corresponding heat generation rate calculated from the electrochemical-thermal coupled model is used.

Although boiling heat transfer facilitates very high heat dissipation rates, it may not prevent onset of thermal runaway under certain circumstances. Since heat dissipation rates from the cell surface depend on both conduction within the cell and convection from cell surface to the coolant, high thermal resistance within the cell may limit the overall heat transfer from the cell to boiling water. As a result, the core temperature of the cell may increase to the threshold value to trigger thermal runaway. One such case is presented in Fig. 11. In Fig. 11, cell thickness is increased to 15 mm, which increases the total thermal resistance of the cell. Under the same conditions as considered in Fig. 10, the thicker cell shows drastically different behavior. Both forced convection and thermal management based on boiling in minichannel are considered. Unlike the results presented in Fig. 10, the cell experiences thermal runaway even when boiling in minichannel is considered as the cooling mechanism. The increased thermal resistance of the cell causes the core temperature of the cell to exceed the threshold value to trigger chain reactions. As a result, the cell ultimately enters thermal runaway. The solid line represents the core temperature, whereas the dashed line shows the surface temperature. Under forced convection, as soon as thermal runaway initiates, the surface temperature of the cell also increases dramatically. This could potentially heat up the neighboring cells leading to the propagation of thermal runaway in the battery module. On the other hand, for the boiling in minichannel case, the increase in core temperature during thermal runaway isn't followed by substantial increase in surface temperature. The high heat dissipation rate from the cell surface to the boiling water keeps the surface

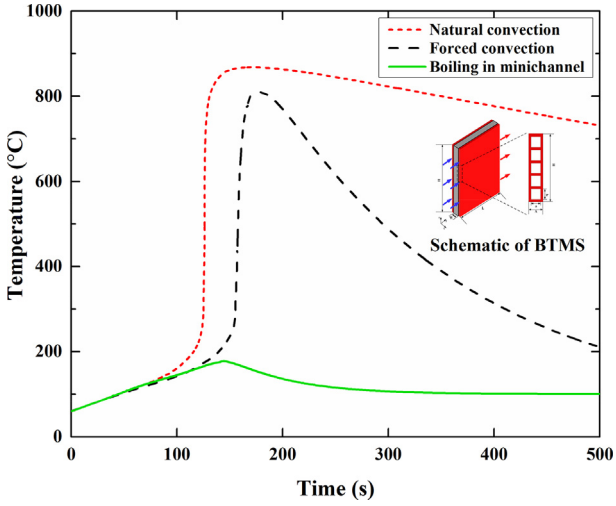

Fig. 10. Evolution of core temperature with time for the cell under different cooling conditions at 25C discharge rate.

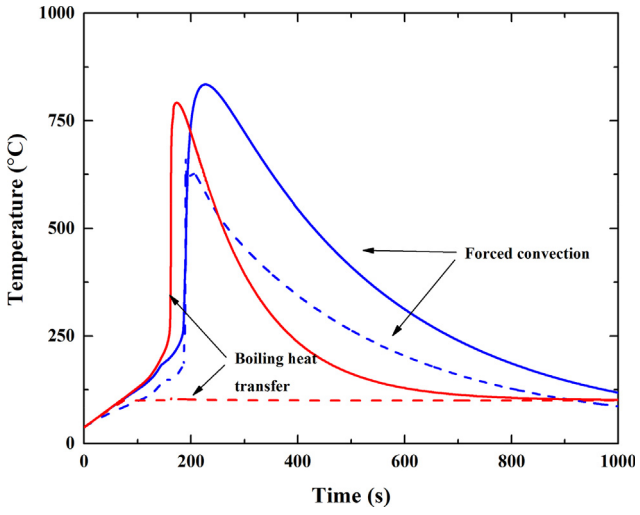

Fig.11. The core (Solid line) and surface (Dashed line) temperature evolution with time for the 15 mm thick cell under forced convection (Blue) and boiling heat transfer in minichannels (Red). (For interpretation of the references to colour in this figure legend, the reader is referred to the web version of this article.)

temperature of the cell from blowing up drastically. This can be very useful in preventing the propagation of thermal runaway to the neighboring cells. The pressure drop in the minichannel can be very large during boiling, which hasn't been analyzed in this study.

5. Conclusion

An analytical thermal runaway model for prismatic and pouch Li-ion cells has been developed. The model has been validated against experiments from literature. Theeffects of key parameters of practical significance, such as discharge rate, ambient temperature, cell thermal conductivity, and cell thickness on the thermal runaway characteristics of the cell have been analyzed. Safe operating conditions in terms of discharge rate, ambient temperature, and convective cooling condition have been determined using the model. It has been found that even a small reduction in the out of plane thermal resistance by enhancing out of plane thermal conductivity and/or reducing cell thickness can dramatically improve the safety of the cell. Further, a thermal runaway prevention strategy utilizing boiling heat transfer in water-cooled minichannel based thermal management as a heat dissipation mechanism has been investigated using the model. Using the model, effectiveness of this thermal runaway prevention strategy has been demonstrated. It has been found that such a strategy can be a viable option to prevent the propagation of thermal runaway at the pack level. This also demonstrates the versatility and capability of the model in analyzing the effects of complex strategies for the thermal runaway prevention purposes.

Acknowledgements

This research was supported by National Science Foundation (No. 1637370), Fundamental Research Funds for the Central Universities (2018JBZ108) and National Natural Science Foundation of China (No. 51776015). This work was performed when one of the authors (Z. An) studied at University of California Merced as a visiting student.

Appendix A. Supplementary material

Supplementary data to this article can be found online at https://doi.org/10.1016/j.applthermaleng.2019.113960.

References

[1] Z. An, L. Jia, Y. Ding, C. Dang, X. Li, A review on lithium-ion power battery thermal management technologies and thermal safety, J. Therm. Sci. 26 (2017) 391–412.
[2] K. Shah, V. Vishwakarma, A. Jain, Measurement of multiscale thermal transport phenomena in Li-Ion cells: a review, J. Electrochem. Energy Convers. Storage 13 (2016) 1–13.
[3] H. Liu, Z. Wei, W. He, J. Zhao, Thermal issues about Li-ion batteries and recent progress in battery thermal management systems: a review, Energy Convers. Manage. 150 (2017) 304–330.
[4] T.M. Bandhauer, S. Garimella, T.F. Fuller, A critical review of thermal issues in Lithium-Ion batteries, J. Electrochem. Soc. 158 (2011) R1–R25.
[5] S. Abada, G. Marlair, A. Lecocq, M. Petit, V. Sauvant-Moynot, F. Huet, Safety focused modeling of lithium-ion batteries: a review, J. Power Sources 306 (2016) 178–192.
[6] X. Feng, M. Ouyang, X. Liu, L. Lu, Y. Xia, X. He, Thermal runaway mechanism of lithium ion battery for electric vehicles: a review, Energy Storage Mater. 10 (2018) 246–267.
[7] T.D. Hatchard, D.D. MacNeil, A. Basu, J.R. Dahn, Thermal model of cylindrical and prismatic Lithium-Ion cells, J. Electrochem. Soc. 148 (2001) A755.
[8] R. Spotnitz, J. Franklin, Abuse behavior of high-power, lithium-ion cells, J. Power Sources 113 (2003) 81–100.
[9] B. Mao, H. Chen, Z. Cui, T. Wu, Q. Wang, Failure mechanism of the lithium ion battery during nail penetration, Int. J. Heat Mass Transf. 122 (2018) 1103–1115.
[10] R. Zhao, J. Liu, J. Gu, A comprehensive study on Li-ion battery nail penetrations and the possible solutions, Energy 123 (2017) 392–401.
[11] P. Peng, Y. Sun, F. Jiang, Thermal analyses of LiCoO2 lithium-ion battery during oven tests, Heat Mass Transf. 50 (2014) 1405–1416.
[12] E. Sahraei, J. Campbell, T. Wierzbicki, Modeling and short circuit detection of 18650 Li-ion cells under mechanical abuse conditions, J. Power Sources 220 (2012) 360–372.
[13] E. Sahraei, R. Hill, T. Wierzbicki, Calibration and finite element simulation of pouch lithium-ion batteries for mechanical integrity, J. Power Sources 201 (2012) 307–321.
[14] D. Ren, X. Feng, L. Lu, M. Ouyang, S. Zheng, J. Li, X. He, An electrochemical-thermal coupled overcharge-to-thermal-runaway model for lithium ion battery, J. Power Sources 364 (2017) 328–340.
[15] A. Kriston, A. Pfrang, H. Döring, B. Fritsch, V. Ruiz, I. Adanouj, T. Kosmidou, J. Ungeheuer, L. Boon-Brett, External short circuit performance of Graphite-LiNi 1/3 Co 1/3 Mn 1/3 O 2 and Graphite-LiNi 0.8 Co 0.15 Al 0.05 O 2 cells at different external resistances, J. Power Sources 361 (2017) 170–181.
[16] X. Feng, J. Sun, M. Ouyang, F. Wang, X. He, L. Lu, H. Peng, Characterization of penetration induced thermal runaway propagation process within a large format lithium ion battery module, J. Power Sources 275 (2015) 261–273.
[17] O.S. Mendoza-Hernandez, H. Ishikawa, Y. Nishikawa, Y. Maruyama, M. Umeda, Cathode material comparison of thermal runaway behavior of Li-ion cells at different state of charges including over charge, J. Power Sources 280 (2015) 499–504.
[18] X. Feng, M. Fang, X. He, M. Ouyang, L. Lu, H. Wang, M. Zhang, Thermal runaway features of large format prismatic lithium ion battery using extended volume accelerating rate calorimetry, J. Power Sources 255 (2014) 294–301.
[19] G.-H. Kim, A. Pesaran, R. Spotnitz, A three-dimensional thermal abuse model for lithium-ion cells, J. Power Sources 170 (2007) 476–489.
[20] K.-C. Chiu, C.-H. Lin, S.-F. Yeh, Y.-H. Lin, K.-C. Chen, An electrochemical modeling of lithium-ion battery nail penetration, J. Power Sources 251 (2014) 254–263.
[21] C. Zhang, S. Santhanagopalan, M.A. Sprague, A.A. Pesaran, Coupled mechanical-electrical-thermal modeling for short-circuit prediction in a lithium-ion cell under mechanical abuse, J. Power Sources 290 (2015) 102–113.
[22] T.G. Zavalis, M.r. Behm, G.r. Lindbergh, Investigation of short-circuit scenarios in a lithium-ion battery cell, J. Electrochem. Soc. 159 (2012) A848.
[23] G. Guo, B. Long, B. Cheng, S. Zhou, P. Xu, B. Cao, Three-dimensional thermal finite element modeling of lithium-ion battery in thermal abuse application, J. Power Sources 195 (2010) 2393–2398.
[24] K. Smith, G.-H. Kim, E. Darcy, A. Pesaran, Thermal/electrical modeling for abuse-tolerant design of lithium ion modules, Int. J. Energy Res. 34 (2010) 204–215.
[25] S.J. Drake, M. Martin, D.A. Wetz, J.K. Ostanek, S.P. Miller, J.M. Heinzel, A. Jain, Heat generation rate measurement in a Li-ion cell at large C-rates through temperature and heat flux measurements, J. Power Sources 285 (2015) 266–273.
[26] T. Grandjean, A. Barai, E. Hosseinzadeh, Y. Guo, A. McGordon, J. Marco, Large format lithium ion pouch cell full thermal characterisation for improved electric vehicle thermal management, J. Power Sources 359 (2017) 215–225.
[27] T. Dong, P. Peng, F. Jiang, Numerical modeling and analysis of the thermal behavior of NCM lithium-ion batteries subjected to very high C-rate discharge/charge operations, Int. J. Heat Mass Transf. 117 (2018) 261–272.
[28] Z. An, K. Shah, L. Jia, Y. Ma, A parametric study for optimization of minichannel based battery thermal management system, Appl. Therm. Eng. 154 (2019) 593–601.
[29] W.B. Gu, C.Y. Wang, Thermal-electrochemical modeling of battery systems, J. Electrochem. Soc. 147 (2000) 2910–2922.
[30] L. Rao, J. Newman, Heat-generation rate and general energy balance for insertion battery systems, J. Electrochem. Soc. 144 (1997) 2697–2704.
[31] Z. An, L. Jia, L. Wei, C. Dang, Q. Peng, Investigation on lithium-ion battery electrochemical and thermal characteristic based on electrochemical-thermal coupled model, Appl. Therm. Eng. 137 (2018) 792–807.
[32] M. Xu, Z. Zhang, X. Wang, L. Jia, L. Yang, A pseudo three-dimensional

electrochemical–thermal model of a prismatic LiFePO4 battery during discharge process, Energy 80 (2015) 303–317.
[33] Y.S. Ye, Lip Huat, Shi Yixiang, Somasundaram Karthik, Andrew A.O. Tay, Effect of thermal contact resistances on fast charging of large format lithium ion batteries, Electrochim. Acta 134 (2014) 327–337.
[34] P. Peng, F. Jiang, Thermal safety of lithium-ion batteries with various cathode materials: a numerical study, Int. J. Heat Mass Transf. 103 (2016) 1008–1016.
[35] C.F. Lopez, J.A. Jeevarajan, P.P. Mukherjee, Characterization of lithium-ion battery thermal abuse behavior using experimental and computational analysis, J. Electrochem. Soc. 162 (2015) A2163–A2173.
[36] K. Shah, A. Jain, Prediction of thermal runaway and thermal management requirements in cylindrical Li-ion cells in realistic scenarios, Int. J. Energy Res. 43 (2019) 1827–1838.
[37] W. Li, Z. Wu, A general correlation for evaporative heat transfer in micro/mini-channels, Int. J. Heat Mass Transf. 53 (2010) 1778–1787.
[38] S.J. Bazinski, X. Wang, Experimental study on the influence of temperature and state-of-charge on the thermophysical properties of an LFP pouch cell, J. Power Sources 293 (2015) 283–291.
[39] M.B. Ahmed, S. Shaik, A. Jain, Measurement of radial thermal conductivity of a cylinder using a time-varying heat flux method, Int. J. Therm. Sci. 129 (2018) 301–308.
[40] V. Vishwakarma, C. Waghela, Z. Wei, R. Prasher, S.C. Nagpure, J. Li, F. Liu, C. Daniel, A. Jain, Heat transfer enhancement in a lithium-ion cell through improved material-level thermal transport, J. Power Sources 300 (2015) 123–131.
[41] A. Gaitonde, A. Nimmagadda, A. Marconnet, Measurement of interfacial thermal conductance in Lithium ion batteries, J. Power Sources 343 (2017) 431–436.
[42] E.W. Lemmon, M.L. Huber, M.O. McLinden, NIST Standard Reference Database 23: Reference Fluid Thermodynamic and Transport Properties-REFPROP, Version 9.1, National Institute of Standards and Technology, Standard Reference Data Program, Gaithersburg, 2013. See < http://www.nist.gov/srd/nist23.cfm > .